Kinetic simulations of x-line expansion in 3D reconnection

Giovanni Lapenta,[1] D. Krauss-Varban,[2] H. Karimabadi,[3] J. D. Huba,[4] L. I. Rudakov,[5] and Paolo Ricci[6]

Received 10 November 2005; revised 24 January 2006; accepted 12 April 2006; published 24 May 2006.

[1] The dynamics of x-line formation and evolution in 3D magnetic reconnection is studied using a fully kinetic approach. An x-line of small length is initialized using a perturbation localized in the current direction. The electrons and ions drift diamagnetically along the current direction of the initial x-line and are further accelerated by the reconnection electric field. The electron and ion motion is in opposite directions and each species extends one end of the x-line. Several predictions based on this picture are formulated and studied and confirmed under parameter variation. Expansion can proceed at a significant fraction of the Alfvén speed, in both directions. **Citation:** Lapenta, G., D. Krauss-Varban, H. Karimabadi, J. D. Huba, L. I. Rudakov, and P. Ricci (2006), Kinetic simulations of x-line expansion in 3D reconnection, *Geophys. Res. Lett.*, *33*, L10102, doi:10.1029/2005GL025124.

1. Introduction

[2] Magnetic field line reconnection is an ubiquitous process in laboratory, space and astrophysical plasmas. It alters the magnetic field topology and can rapidly transfer energy from the magnetic field to the plasma. In the classic 2D picture, reconnection progresses through the formation of a dissipation region around an x-point, where the field lines break and reconnect. This configuration has been extensively studied with a variety of simulation codes, e.g., through the GEM challenge [*Birn et al.*, 2001]. In simulations that contain at least some ion-kinetic physics, it is found that the plasma enters the reconnection region at approximately 0.1 V_A (V_A is the Alfvén speed) and exits the regions highly accelerated at close to V_A.

[3] Details of the reconnection process can be dramatically different in 2D and 3D. One of the important 3D effects, that is of theoretical and observational interest, is the question of the process and the rate at which the x-line grows in the third direction along the current. Reconnection can be induced by large scale ordered processes or instabilities (e.g., the tearing mode), producing a finite size x-line from the outset. Or, reconnection may be initiated by localized processes or perturbations, leading to an initially short x-line which might progress by expanding or by merging with other x-lines. Here we bypass the reconnection onset and the initial formation of the x-line and instead focus on the question of the mechanism and the speed at which the x-line spreads in the third direction. This issue has direct relevance to understanding and quantifying reconnection in the magnetotail, at the magnetopause, and in other space physics settings.

[4] Relatively uninhibited and fast expansion of the x-line would allow widespread reconnection in the 3rd direction. In the context of solar wind - magnetosphere interaction it is imperative to note that, at any given x-line, the total amount of reconnected flux and solar wind plasma entry into the magnetosphere is directly proportional to the length of the x-line.

[5] Indeed, there is multi-spacecraft evidence that at least at times the x-line can extend over several Earth radii at the magnetopause [*Phan et al.*, 2000]. Ground-based observations and satellite-based auroral imaging also support that the x-line can stretch over most of the dayside magnetopause [*Fuselier et al.*, 2002]. In the solar wind, x-line extending hundreds of Earth radii have been identified [*Phan et al.*, 2006].

[6] To date, there have only been a limited number of investigations assessing reconnection dynamics in the third direction. *Huba and Rudakov* [2002] performed a 3D study using the NRL Hall MHD code VooDoo [*Huba*, 2003]. They found that a reconnection x-line formed from localized perturbation propagates in the direction of electron flow. They attributed this to a 'reconnection wave' that propagates at a velocity $V_e \simeq J/ne$ if the electrons carry the current. *Shay et al.* [2003] have suggested that the x-line could expand in the ion direction if the ions carried the current. 3D hybrid simulations have indicated that the x-line propagates in both the electron and ion direction [*Karimabadi et al.*, 2004]. However, in hybrid simulations the ions typically carry most of the current, while the electrons are frozen to the magnetic field except in regions of explicit resistivity. Not surprisingly, it was found that the x-line only extends to the region where resistivity is present. Fully kinetic 3D simulations have shown the tendency of multiple reconnection sites to merge [*Hesse et al.*, 2001] and of locally driven reconnection to extend following the electron flow [*Pritchett and Coroniti*, 2001].

[7] From the above it is clear that the dynamics of 3D magnetic reconnection should be addressed with both electron and ion kinetic physics properly accounted for. The present study uses a fully kinetic particle simulation code. Thus, it allows for the complete physics and is not subject to fluid approximations or imposed resistivity models. Here, we study with a fully kinetic approach how an initially localized perturbation extends and expands the

[1]Theoretical Division, Los Alamos National Laboratory, Los Alamos, New Mexico, USA.
[2]Space Sciences Laboratory, University of California, Berkeley, California, USA.
[3]Department of Electrical and Computer Engineering, University of California, San Diego, La Jolla, California, USA.
[4]Naval Research Laboratory, Washington, D. C., USA.
[5]Berkeley Scholars, Inc., Springfield, Virginia, USA.
[6]Department of Physics and Astronomy, Dartmouth College, Hanover, New Hampshire, USA.

0094-8276/06/2005GL025124

Table 1. Summary of the Initial Data for the Simulations[a]

Case	m_i/m_e	L/d_i	T_i/T_e	L_x/d_i	L_y/d_i	L_z/d_i
A	25	.5	5	12.8	19.2	6.4
B	180	.5	5	12.8	19.2	6.4
C	25	1.3	5	32	48	16
D	25	.5	1/5	12.8	19.2	6.4
E	180	.5	1/5	12.8	19.2	6.4
F	1	.7	1	18	13.44	9

[a]Case A is the GEM challenge.

x-line in the 3rd dimension (i.e., in the direction of the current).

2. Equilibrium and Simulation Methods

[8] We consider an equilibrium described by the Harris sheet with a drift velocity u_s and thermal velocity $v_{th,s} = \sqrt{k_B T_s/m_s}$ for species s. The ratio of the ion drift velocity to ion thermal velocity is related to the current sheet thickness L: $u_i/v_{th,i} = 2\rho_i/L$ where ρ_i is the ion gyroradius. The ratio of the drift velocities of the two species is $u_i/u_e = -T_i/T_e$.

[9] The usual geomagnetic reference frame is used with x-axis $[-L_x/2, L_x/2]$ in the magnetic field direction, y-axis $[0, L_y]$ in the current direction and z-axis $[-L_z/2, L_z/2]$ along the gradients of the current and magnetic field. The equilibrium magnetic field is in the x-direction $\mathbf{B}_0(z) = -B_0 \tanh(z/L)\,\mathbf{e}_x$. The corresponding plasma density is $n(z) = n_b + n_0\,\mathrm{sech}^2(z/L)$ where n_0 is the peak plasma density and $n_b = 0.1\,n_0$ is a non-drifting background density that does not contribute to the current. We remark that a Harris current sheet with a background population is a Vlasov equilibrium.

[10] We initialize the system with a 3D magnetic perturbation localized in the y direction (i.e., along the current). The initial perturbation is specified by a perturbed potential vector A_y of the form

$$A_y(x,y,z) = -A_0 \cos(k_x x)\cos(k_z z)\mathrm{sech}\big(k_y(y-y_0)\big) \qquad (1)$$

with $y_0 = L_y/2$, $k_x = 2\pi/L_x$, $k_y = 10/L_y$, $k_z = \pi/L_z$ and $A_0 = \varepsilon B_0 c/\omega_{pi}$. In the simulations below we choose $\varepsilon = 0.4$ unless stated otherwise.

[11] For the field boundary conditions, we extend the typical boundary conditions of the GEM challenge [*Birn et al.*, 2001] (periodic conditions in x and Dirichlet conditions in z) with periodic conditions in y. Similarly, the particles are reflect at the z boundaries and periodic boundary conditions are applied in x and y.

[12] The Vlasov-Maxwell system described above is simulated using CELESTE3D [*Brackbill and Forslund*, 1985; *Lapenta et al.*, 2006]. CELESTE3D is based on the implicit moment method that removes the Courant conditions associated with the speed of light and electron plasma waves; it thereby allows time steps far exceeding the typical time steps used in explicit PIC simulations [*Brackbill and Forslund*, 1985]. The finite grid instability is also reduced drastically and much larger cells are allowed than in typical explicit PIC codes.

[13] In the present simulations the electron gyroscale is resolved using a time step $\omega_{ce}\Delta t = 0.3$. We resolve the ion skin depth using a grid spacing in every direction $\Delta = 0.2\,d_i$. For the simulations described below with mass ratio $m_i/m_e = 1$ and $m_i/m_e = 25$ we resolve also the electron skin depth: $\Delta/d_e = 0.2$ and $\Delta/d_e = 0.45$, respectively. In the two simulations described below with $m_i/m_e = 180$, we still resolve the electron gyrofrequency and the ion skin depth as above, but the electron skin depth is not resolved, $\Delta/d_e \approx 2$. (In a previous study, a detailed comparison with the massively parallel explicit 2D PIC code NPIC demonstrated that CELESTE3D captures sub-grid level physics using the particle information through the implicit moment method [*Ricci et al.*, 2004].) We use typically 27 particles per species per cell to describe the Harris equilibrium and 8 particles per species per cell to describe the non-drifting background. The same number of particles per cell is used everywhere in the domain, assigning particle weights according to local density.

3. Mechanism of X-Line Expansion

[14] We have conducted a number of simulations varying several equilibrium parameters: the current sheet thickness, the velocity ratio of the two species, and the mass ratio of the two species. Table 1 summarizes the parameters of all simulations. The initial magnetic perturbation determines the initially finite length of the x-line. As the system evolves, the x-line can expand in both directions depending on the physical conditions.

[15] To illustrate the configuration of the x-line and the reconnection region around it, we have designed the following diagnostic. The figures shown below are produced by first detecting at what value $z = \mathbb{Z}(x, y)$ the magnetic field component B_x reverses direction for each vertical line with a given x and y. This determines a surface $\mathbb{Z}$ defined as $(x, y, \mathbb{Z}(x, y)) \in \mathbb{R}^3$ where $B_x = 0$ which can be mapped to the (x,y) plane. We label the direction normal to the surface n and the tangential direction orthogonal to the y direction as t. The reason for resorting to this approach is linked to the drift-kink and Kelvin-Helmholtz instabilities. Previous work [*Lapenta and Brackbill*, 2002; *Scholer et al.*, 2003] has shown that unlike reduced models, the full kinetic model is subject to a host of current aligned instabilities that lead to a flapping of the current sheet similar to that observed in the earth's magnetotail [*Sergeev et al.*, 2003]. In studying the behavior of the x-line we need to remove the effects of current sheet flapping that tends to warp all physical quantities out of the $z = 0$ plane. By computing the surface $\mathbb{Z}$ we remove the effect of flapping.

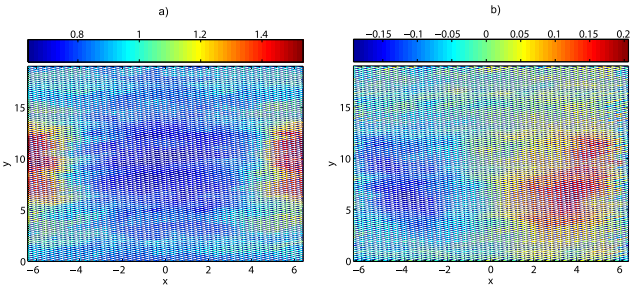

Figure 1. (a) Ion density and (b) normal magnetic field B_n on the $Z(x, y)$ surface at time $\omega_{ci}t = 3$ for case E.

Table 2. Summary of the Velocity of the Ends of the X-Line u_+ (Top End) and u_- (Bottom End) and of the Species Velocities u_{e0}, u_{i0} (Electrons and Ions) in the Initial State and Once the Reconnection Region is Formed u_{eR}, u_{iR} (Measured at the Output From the X-Line)[a]

Case	u_{e0}/V_A	u_{i0}/V_A	u_{eR}/V_A	u_{iR}/V_A	u_+/V_A	u_-/V_A
A	−.33	1.67	−1.16	1.74	1.79	−.22
B	−.33	1.67	−3.1	1.7	.6	−.34
C	−.13	.65	−.7	.6	.08	−.04
D	−5.1	1.0	−2.3	1.1	.35	−.78
E	−1.65	.33	−6.9	.52	0?	−1.47
F	.7	.7	−1.0	1.0	.35	.35

[a]All velocities are normalized to the Alfvén speed V_A defined with the peak field and peak density.

[16] Figure 1 illustrates the diagnostics we use in detecting the extension of the x-line at a given time. Figure 1a shows the ion density on the $\mathbb{Z}$ surface projected on the (x, y) plane at time $\omega_{ci}t = 3$ for case E (similar results are obtained in all cases). The current sheet is thinner and the density is depleted only in a limited section of the y axis around the x-line where reconnection is occurring. In the same segment of the y axis, the density is increased near the o-points. Around the x-line, a signature of reconnection is the reversal of the component of the magnetic field normal to $\mathbb{Z}$ surface, B_n (see Figure 1b). The reversal of the B_n component corresponds to the segment of the y axis where the x-line has formed. The diagnostic relative to B_n agrees with that of density depletion. Other classic signatures of reconnection (e.g., ion and electron outflow velocity v_{et}, v_{it}, not shown here) confirm the same conclusion.

[17] An additional clear feature of the reconnection region is the acceleration along the y direction of ions and electrons in the reconnection region. In the reconnection region the electrons are strongly accelerated while the ions are accelerated by a much smaller factor. The acceleration is determined by the reconnection electric field that is in the y direction and can accelerate electrons and ions once they become demagnetized in their respective dissipation region (which is different for ions and electrons, being of size $\delta = d_i$ for the ions and $\delta_e = \sqrt{\rho_e L}$ for the electrons).

[18] Unlike the fluid model, in the kinetic equilibrium, the two species carry a current by actually drifting diamagnetically in the y direction. The ratio of the ion and electron diamagnetic drift is directly proportional to the temperature ratio but of opposite sign: $u_{e0}/u_{i0} = -T_{e0}/T_{i0}$. The ions and electrons drift in opposite direction and with a speed proportional to their temperature. The initial velocities along y are listed in Table 2. In the reconnection region the ions and electrons are further accelerated by the reconnection field and their maximum speeds in the reconnection region are listed in Table 2.

[19] The species drift has a profound effect on the extension of the x-line by forming the shock-like features observed in Figure 1. As the initial perturbation, localized in the center of the y axis leads to a thinner, more rarefied, layer in that localized region, the ion and electron flow will carry that thinning along the y axis. As the thinning is extended along the y axis, effectively the initial perturbation is carried along, carrying reconnection with it. We note that the ions are not magnetized in the current layer and do not directly carry field lines, but still carry the density depletion that triggers the onset of reconnection [*Huba and Rudakov*, 2003].

[20] Simply put, the ions and electrons carry the x-line with them. At each end, the ions cross the end of the x-line moving forward, the electrons moving backward. At the forward end, the ions move forward carrying the thinning, while the electrons move into the reconnection region and are carried away by the reconnection jets along the x-axis. The ion motion carries the rarefaction region forward, advancing the current thinning and the x-line forward. Conversely, at the back end the ions move into the reconnection region, and the electron extend the rarefaction in the backward direction, extending the x-line backward [*Huba and Rudakov*, 2002].

4. Simulation Results

[21] To investigate the extension of the x-line in the y direction, we study three typical signatures of reconnection: the 'out-of-plane' component of the magnetic field B_n that changes sign at the x-line, the outflow of electrons at super-Alfvénic speeds from the reconnection region and the outflow of ions at Alfvénic speeds. We measure each of these 3 quantities on the surface $\mathbb{Z}$ defined above. We compute the first and second moment of each distribution:

$$\langle y \rangle = \frac{\int_{\mathbb{Z}} |\psi(x,y)| y dS}{\int_{\mathbb{Z}} |\psi(x,y)| dS}$$
$$\langle y^2 \rangle = \frac{\int_{\mathbb{Z}} |\psi(x,y)| (y - \langle y \rangle)^2 dS}{\int_{\mathbb{Z}} |\psi(x,y)| dS} \quad (2)$$

where ψ is a scalar field. Assuming uniformity along the x-line, the extension of the x-line can be computed easily from the first two moments:

$$y^{\pm} = \langle y \rangle \pm \frac{3}{2} \sqrt{\langle y^2 \rangle} \quad (3)$$

We define the extrema of the x-line as the results of averaging the extrema computed with the scheme just described for each of the 3 quantities: B_n, u_{et} or u_{it}. We have verified that the 3 diagnostics give consistent results and we take the average to reduce noise.

[22] As an example of this procedure, Figure 2 shows the evolution of the x-line for case D. The initial perturbation does not immediately lead to reconnection. As in the GEM challenge, an initial phase of adjustment is followed by the appearance of strong signatures of reconnection. The onset of fast reconnection and the initial formation of the x-line correspond to an initial reduction in the variance of the diagnostics defined in equation (2) and is seen in Figure 2 as the initial concentration of the ends of the forming x-line. Only after the initial adjustment is finished, the x-line starts to extend. In case D, the initial phase lasts less than $\omega_{ci}t < 1$, and similar behavior (with a variation in the duration of the initial phase) is observed in all other cases not shown. In all

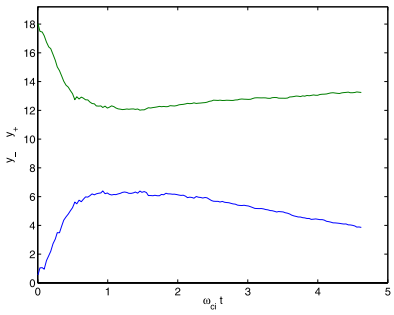

Figure 2. Evolution of the upper (y^+) and lower (y^-) ends of the x-line for case D.

cases the velocity of extension of the ends of the x-line is measured after the end of the initial phase.

[23] We repeated the same analysis for all cases A-F obtaining similar figures that we do not show here. Instead, we report the final result, the velocity of extension of each end of the x-line in Table 2. For reference, we also list the unperturbed initial velocity for each species, and the maximum speed reached by each species in the reconnection region.

5. Discussion

[24] A number of conclusions can be reached based on the phenomenological interpretation of the process of x-line extension. First, the x-line extends in the direction of the current carrier. If electrons are the dominant current carrier ($u_e \gg u_i$) then the x-line extends only in the direction of electron flow; if ions are the dominant current carrier ($u_i \gg u_e$) then the x-line extends only in the direction of ion flow. In the case of an electron-positron plasma with equal temperatures, the x-line expands symmetrically in both directions. Second, when the current sheet thickness is increased, it becomes harder for ions and electrons to extend the thin reconnection region into the thick unperturbed current layer. The speed of the x-line expansion progressively becomes a smaller fraction of the ion and electron flow speeds. This is consistent with the results of *Huba and Rudakov* [2003] who describe the impact of a density gradient along the current direction on reconnection dynamics. Third, as the mass ratio is changed, the electron and ion acceleration in the reconnection region changes [*Ricci et al.*, 2003]; the electrons are accelerated to higher speeds increasing their ability to move the field lines. The consequence of this trend is that the electrons are more effective in moving the back end of the x-line as the mass ratio is increased. To prove this point, besides comparing case A with case B and case D with case E, we have also conducted a parametric study for a current sheet with $L/d_i = 1$ and $T_i/T_e = 5$, varying the mass ratio: 25,50,100,200. The velocity of the upper end is essentially unmodified: the velocity in the four cases is respectively $u_+ = .36, .38, .33$ and $.32$. The changes observed are not a clear trend and are below the accuracy of the detection method. But for the back end, where the electron carry the x-line backward, the velocity scales strongly with the mass ratio, increasing as the electrons become lighter and are accelerated more in the reconnection region: $u_- = -.29, -.34, -.44$ and $-.76$.

[25] Asymmetries between ion and electron motion (and the respective x-line end sides) could have far-reaching consequences. For example, GEOTAIL [*Miyashita et al.*, 2000] and WIND [*Raj et al.*, 2002] statistical studies have indicated a dawn-dusk asymmetry of reconnection signatures in the magnetotail, consistent with the ion direction of motion. Also, such asymmetries could be both due to x-line development or preferred initial x-line location. Moreover, because of momentum, current-carrying ions tend to transport reconnection signatures with them outside of the diffusion region proper [*Karimabadi et al.*, 2004] – a large-scale effect that is outside the scope of work presented here and will be considered in a future article.

[26] **Acknowledgment.** Support for GL is provided by the LDRD program at LANL and by the United States Department of Energy, under contract W-7405-ENG-36. Support for JDH was provided by ONR and NASA, support for DKV by NASA grant NNG04GH38G, and support for HK by NSF grant ATM-9901665.

References

Birn, J., et al. (2001), Geospace environmental modeling (GEM) magnetic reconnection challenge, *J. Geophys. Res.*, *106*, 3715–3719.

Brackbill, J. U., and D. W. Forslund (1985), Simulation of low-frequency, electromagnetic phenomena in plasmas, in *Multiple Time Scales*, pp. 377–395, edited by J. U. Brackbill and B. I. Cohen, Elsevier, New York.

Fuselier, S. A., H. U. Frey, K. J. Trattner, S. B. Mende, and J. L. Burch (2002), Cusp aurora dependence on interplanetary magnetic field B_z, *J. Geophys. Res.*, *107*(A7), 1111 doi:10.1029/2001JA900165.

Hesse, M., M. Kuznetsova, and J. Birn (2001), Particle-in-cell simulations of three-dimensional collisionless magnetic reconnection, *J. Geophys. Res.*, *106*(A12), 29,831–29,842.

Huba, J. (2003), *Space Plasma Simulation*, Springer, New York.

Huba, J., and L. Rudakov (2002), Three dimensional Hall magnetic reconnection, *Phys. Plasmas*, *9*, 4435–4438.

Huba, J., and L. Rudakov (2003), Hall magnetohydrodynamics of neutral layers, *Phys. Plasmas*, *10*, 3139–3150.

Karimabadi, H., D. Krauss-Varban, J. D. Huba, and H. X. Vu (2004), On magnetic reconnection regimes and associated three-dimensional asymmetries: Hybrid, Hall-less hybrid, and Hall-MHD simulations, *J. Geophys. Res.*, *109*, A09205, doi:10.1029/2004JA010478.

Lapenta, G., and J. Brackbill (2002), Nonlinear evolution of the lower hybrid drift instability: Current sheet thinning and kinking, *Phys. Plasmas*, *9*(5), 1544–1554.

Lapenta, G., J. Brackbill, and P. Ricci (2006), Kinetic approach to microscopic-macroscopic coupling in fusion plasmas, *Phys. Plasmas*, *13*, 055904.

Miyashita, Y., S. Machida, T. Mukai, Y. Saito, K. Tsuruda, H. Hayakawa, and P. Sutcliffe (2000), A statistical study of variations in the near and middistant magnetotail associated with substorm onsets: Geotail observations, *J. Geophys. Res.*, *105*, 15,913–15,930.

Phan, T. D., et al. (2000), Extended magnetic reconnection at the Earth's magnetopause from detection of bi-directional jets, *Nature*, *404*, 848–850.

Phan, T. D., et al. (2006), A magnetic reconnection X-line extending more than 390 Earth radii in the solar wind, *Nature*, *439*, 175–178.

Pritchett, P. L., and F. V. Coroniti (2001), Kinetic simulations of 3D reconnection and magnetotail disruptions, *Earth Planets Space*, *53*, 635–643.

Raj, A., T. Phan, R. P. Lin, and V. Angelopoulos (2002), Wind survey of high-speed bulk flows and field-aligned beams in the near-Earth plasma sheet, *J. Geophys. Res.*, *107*(A12), 1419, doi:10.1029/2001JA007547.

Ricci, P., G. Lapenta, and J. Brackbill (2003), Electron acceleration and heating in collisionless magnetic reconnection, *Phys. Plasmas*, *10*(9), 3554–3560.

Ricci, P., J. Brackbill, W. Daughton, and G. Lapenta (2004), Collisionless magnetic reconnection in the presence of a guide field, *Phys. Plasmas*, *11*(8), 4102–4114.

Scholer, M., I. Sidorenko, C. H. Jaroschek, P. A. Treumann, and A. Zeiler (2003), Onset of collisionless magnetic reconnection in thin current sheets: Three-dimensional particle simulations, *Phys. Plasmas*, *10*, 3521–3527.

Sergeev, V., et al. (2003), Current sheet flapping motion and structure observed by Cluster, *Geophys. Res. Lett.*, *30*(6), 1327, doi:10.1029/2002GL016500.

Shay, M. A., J. F. Drake, M. Swisdak, W. Dorland, and B. N. Rogers (2003), Inherently three dimensional magnetic reconnection: A mechanism for bursty bulk flows?, *Geophys. Res. Lett.*, *30*(6), 1345, doi:10.1029/2002GL016267.

J. D. Huba, Naval Research Laboratory, Code 6790, Washington, DC 20375, USA.

H. Karimabadi, Department of Electrical and Computer Engineering, University of California, San Diego, La Jolla, CA 92093, USA.

D. Krauss-Varban, Space Sciences Laboratory, University of California, Berkeley, CA 94720, USA.

G. Lapenta, Los Alamos National Laboratory, Los Alamos, NM 87545, USA. (lapenta@lanl.gov)

P. Ricci, Department of Physics and Astronomy, Dartmouth College, Hanover, NH 03755, USA.

L. I. Rudakov, Berkeley Scholars, Inc., P.O. Box 852, Springfield, VA 22150, USA.